Nernst Effect of High-Mobility Weyl Electrons in NdAlSi Enhanced by a Fermi Surface Nesting Instability

Rinsuke Yamada,[1,*] Takuya Nomoto,[2] Atsushi Miyake,[3] Toshihiro Terakawa,[1] Akiko Kikkawa,[4] Ryotaro Arita,[2,4] Masashi Tokunaga,[3] Yasujiro Taguchi,[4] Yoshinori Tokura,[1,4,5] and Max Hirschberger[1,4,†]

[1]*Department of Applied Physics, The University of Tokyo, Bunkyo-ku, Tokyo 113-8656, Japan*
[2]*Research Center for Advanced Science and Technology, The University of Tokyo, Komaba, Tokyo 153-8904, Japan*
[3]*The Institute for Solid State Physics, The University of Tokyo, Kashiwa 277-8581, Japan*
[4]*RIKEN Center for Emergent Matter Science (CEMS), Wako, Saitama 351-0198, Japan*
[5]*Tokyo College, The University of Tokyo, Bunkyo-ku, Tokyo 113-8656, Japan*

(Received 23 July 2023; revised 31 January 2024; accepted 5 March 2024; published 16 April 2024)

The thermoelectric Nernst effect of solids converts heat flow to beneficial electronic voltages. Here, using a correlated topological semimetal with high carrier mobility μ in the presence of magnetic fluctuations, we demonstrate an enhancement of the Nernst effect close to a magnetic phase transition. A magnetic instability in NdAlSi modifies the carrier relaxation time on "hot spots" in momentum space, causing a strong band filling dependence of μ. We quantitatively derive electronic band parameters from a novel two-band analysis of the Nernst effect S_{xy}, in good agreement with quantum oscillation measurements and band calculations. While the Nernst response of NdAlSi behaves much like conventional semimetals at high temperatures, an additional contribution ΔS_{xy} from electronic correlations appears just above the magnetic transition. Our work demonstrates the engineering of the relaxation time, or the momentum-dependent self-energy, to generate a large Nernst response independent of a material's carrier density, i.e., for metals, semimetals, and semiconductors with large μ.

DOI: 10.1103/PhysRevX.14.021012

Subject Areas: Condensed Matter Physics, Magnetism, Materials Science

I. INTRODUCTION

Thermoelectric effects convert temperature gradients to useful electric power and are broadly classified into two categories: first, the Seebeck effect, where a voltage is induced parallel to the heat gradient, and second, the Nernst effect, where the voltage appears in a direction perpendicular to the heat flow. While both the Seebeck and Nernst effects of narrow-gap semiconductors have been intensively studied in the context of energy-saving technology for more than two decades [1–3], the further technological potential of Nernst-type phenomena was pointed out recently [4]. The two most well-known contributions to this thermoelectric response are the normal Nernst effect from the orbital motion of electrons and the anomalous Nernst effect that appears in the ground state of magnetic materials, which is typically proportional to the magnetization [5–8]. Here, we highlight a magnetic enhancement of the former effect in a semimetal with high carrier mobility, a consequence of electronic correlations that has been little explored so far.

Thermoelectric phenomena are generally known to be very sensitive to details of the electronic structure in the vicinity of the Fermi energy E_F, which separates occupied from unoccupied quantum states in a solid [9,10]. Specifically, the normal Nernst effect contains terms proportional to the filling-dependent change in carrier density, dn/dE, and terms proportional to the change in carrier relaxation (scattering) time, $d\tau/dE$ (see Sec. III). The dn/dE term drives a large thermoelectric response only in materials with a low number of carriers, such as narrow-gap semiconductors, but the latter effect may largely enhance the thermoelectric response even in good metals [11–18]. One particularly well-established way to enhance band-filling dependence of the relaxation time, $d\tau/dE$, is by electron correlations, especially close to "hot spots," or regions of enhanced scattering, on the electronic Fermi surface [11,19]. Meanwhile, a quantitative demonstration of enhanced Nernst signals from such hot spots has remained an open challenge, largely due to the low carrier mobility of many available correlated materials. To address this issue, we study the

*To whom correspondence should be addressed: ryamada@ap.t.u-tokyo.ac.jp
†To whom correspondence should be addressed: hirschberger@ap.t.u-tokyo.ac.jp

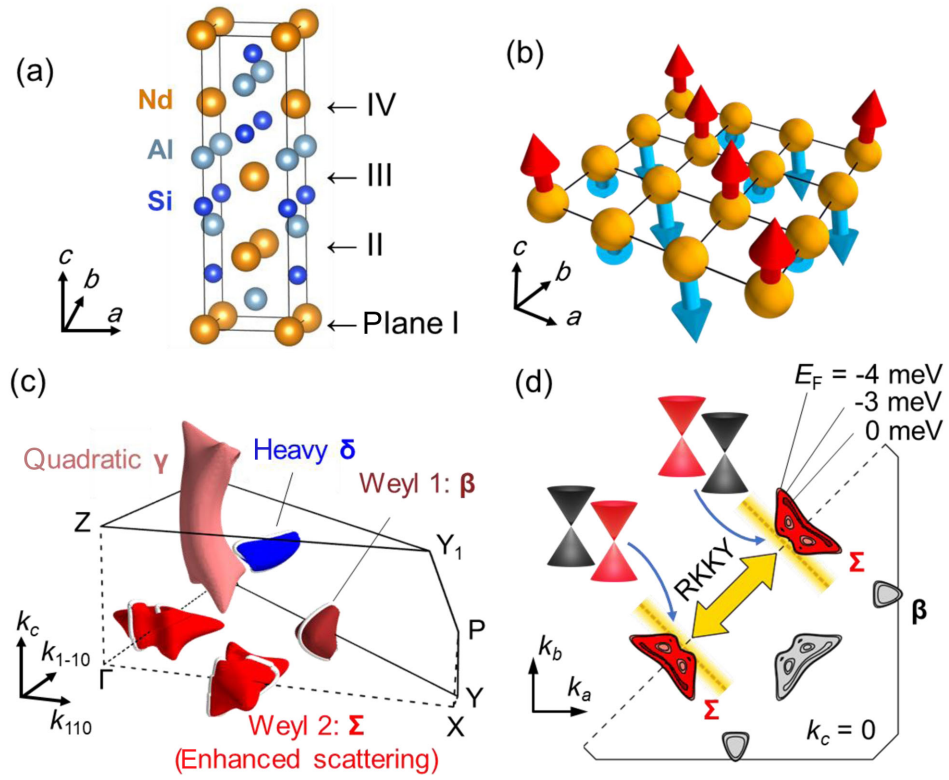

FIG. 1. Fermi surface nesting of Weyl points in NdAlSi. (a) Crystal structure of NdAlSi, with polar c axis. (b) Spin texture in the ab plane (plane I) with the magnetic ordering vector $\mathbf{Q} \approx (2/3, 2/3, 0)$ along the [110] direction, as revealed in Ref. [22]. (c) Electronic structure in NdAlSi; one octant of the Brillouin zone is shown. There are four types of Fermi surfaces: a high-mobility Weyl β pocket (brown), a Weyl Σ pocket subject to Ruderman-Kittel-Kasuya-Yosida (RKKY) interactions (red), a hole γ pocket with quadratic electronic band dispersion (pink), and an electron δ pocket with heavy electron mass (blue). In the Hall and Nernst effects, only the former three contribute dominantly (below). White solid lines indicate the extremal cross sections of electron orbits observed experimentally when a magnetic field is applied along the a axis. (d) Two-dimensional cuts of Fermi surfaces at $k_z = 0$, where traces corresponding to $E_F = -4$, -3, and 0 meV are shown. Yellow lines and a shaded region indicate the nesting plane with ordering vector $\mathbf{Q}$. Illustration: Weyl cones in the electronic band structure of Σ.

Nernst response of the topological semimetal NdAlSi with elevated carrier mobility [20–22] and hot spots of scattering at a Fermi surface nesting instability (Fig. 1). The results indicate that Nernst effects from $d\tau/dE$ become large and dominant in clean systems with highly mobile charge carriers coupled to collective modes, such as lattice waves or—our focus here—magnetic fluctuations.

Topological semimetals, where crystalline or time-reversal symmetries enforce degeneracies of electronic bulk bands and associated surface states in solids [17,20–25], are suitable to demonstrate the proposed Nernst effect from $d\tau/dE$: They have large carrier mobilities μ due to protected band crossings, where the effective band mass approaches zero. Furthermore, their physical behavior can be designed based on symmetry principles, and electron correlations can be introduced by chemical alloying while leaving crystal symmetries and related band crossings intact. Third and finally, transport properties can be studied quantitatively in such materials due to a low number of Fermi surface sheets with high carrier mobility, generating transport behavior that is conveniently nonlinear as a function of magnetic field.

We choose the polar magnetic Weyl semimetals RAlSi/RAlGe (R = rare earth) as promising materials for our proof-of-principle study, where high-mobility Weyl electrons coexist with complex magnetic order at low temperatures [20–22]. In these materials, Weyl fermions [23]—that is, singly degenerate linear band crossing points—are present due to breaking of inversion symmetry in the body-centered tetragonal space group $I4_1md$ [Fig. 1(a)]. Weyl fermions and other topologically protected band degeneracies can be generated in inversion symmetric materials at the magnetic phase transition [24]. In contrast, the electronic structure in polar and chiral topological semimetals is less sensitive to magnetic order and forms a robust backdrop for the study of correlation phenomena [20,21].

Here, we demonstrate that the thermoelectric response of a prototypical magnetic Weyl semimetal, NdAlSi, can be enhanced in the vicinity of a magnetic instability. This correlation phenomenon benefits from the high carrier

mobility of quasirelativistic Weyl electrons, demonstrated here by a thorough analysis of the Nernst effect S_{xy} in the high-temperature regime. Semiclassical transport theory, ignoring electron-electron scattering, also reproduces S_{xy} well at the base temperature of our experiment. Meanwhile, an additional Nernst contribution ΔS_{xy} appears and is strongly enhanced just above the transition to long-range magnetic order at $T_N = 7$ K, where magnetic fluctuations are coupled to the Fermi surface of the electron gas. Through *ab initio* calculations of the electronic structure, as well as careful evaluation of the experimental profile $\Delta S_{xy}(T)$ and its magnitude, we conclude that the additional term originates from the band-filling (energy) derivative of the carrier relaxation time, $d\tau/dE$, due to a magnetic nesting instability between high-mobility Weyl electrons. Finally, the results are placed in the wider context of thermoelectric materials with relaxation time contributions.

II. RESULTS

A. Electric transport and high-mobility charge carriers

The electronic band structure of NdAlSi is composed of several Fermi surfaces; Fig. 1(c) shows the result of our *ab initio* band-theory calculations, combined with the present electric transport experiments (see Supplemental Material [26]). The Fermi surface includes two Weyl-type sheets (β, Σ) with linear band dispersions and two trivial pockets (γ, δ) with rather quadratic bands. Only the δ pocket has electronlike transport characteristics; all others are holelike (Figs. S2 and S3). In this work, we observe strong thermoelectric anomalies due to a Fermi surface nesting instability [27–29] towards a periodically modulated, helimagnetic state with ordering vector $\mathbf{Q} = (2/3, 2/3, 0)$ [see Fig. 1(b) and Ref. [22]]. The ordering vector, shown as a fat yellow arrow in Fig. 1(d), causes strong magnetic scattering of high-mobility Weyl carriers in the Σ pockets above the magnetic ordering temperature. Meanwhile, signatures of charge carriers in the other bands can also be clearly identified in our transport experiments.

We first construct band-theoretical models of the electronic structure in NdAlSi by electrical transport measurements. Here, the electric current J_x, the magnetic field B_z, and the transverse (Hall) electric field E_y define a right-hand Cartesian frame along the x, z, and y axes, respectively; this is shown in Fig. 2(a), inset. The Hall conductivity relates them according to $J_x = \sigma_{xy} E_y$. Field-dependent traces of σ_{xy} show a dispersive shape with a sharp maximum around 2 Tesla, accompanied by pronounced Shubnikov–de Haas oscillations. Our two-carrier Drude fit, shown by black dashed lines in Fig. 2(a), reproduces σ_{xy} well up to room temperature (see Sec. III). Figures 2(b) and 2(c) show electronic band parameters derived from the fit: n_1 and n_2 are positive, reaching values of 6.5×10^{19} cm^{-3} and 2.5×10^{19} cm^3 at low temperature, which indicates coherent metallic conduction. Similar transport parameters are also obtained from the two-carrier fit of σ_{xx} (see Supplemental Material [26]). The carrier mobilities μ_1 and μ_2 rise monotonically upon cooling towards 2000 cm^2/Vs and 6000 cm^2/Vs at 8 K, high values

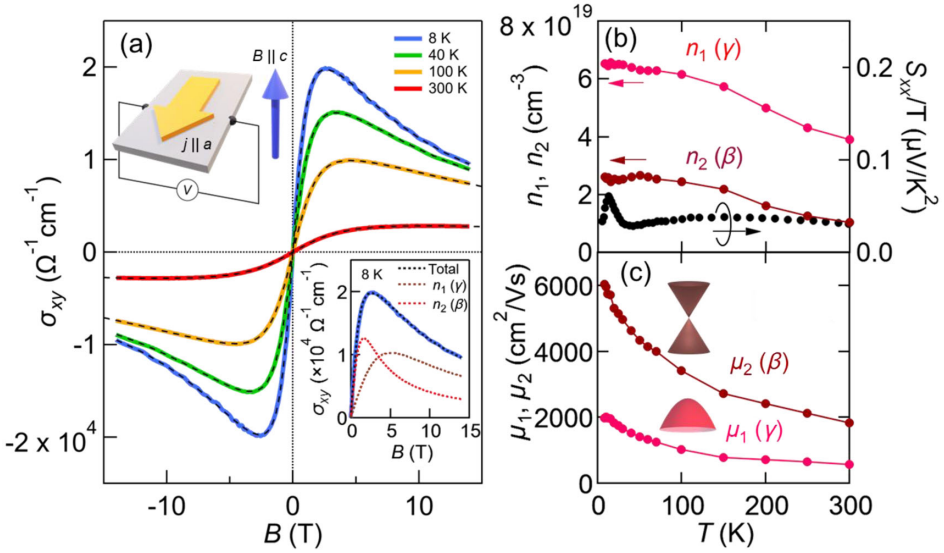

FIG. 2. High-mobility electrons from Weyl and trivial Fermi surface pockets in NdAlSi, detected by electrical transport. (a) Hall conductivity σ_{xy} at various temperatures. The black dashed lines indicate fitting to a two-carrier model. Inset (top left): sample geometry, where magnetic field **B** and electric current **J** are applied along the c axis and a axis, respectively. Inset (bottom): two components of the fit, shown individually. (b) Carrier density of two Fermi surface sheets, estimated by two-carrier fitting (left axis). The parameters μ_1, n_1 are assigned to a trivial (γ) and μ_2, n_2 to a Weyl-type (β) Fermi surface sheet, respectively. Right axis: temperature dependence of the Seebeck effect divided by temperature, with enhancement above T_N likely due to electron correlations on Σ. (c) Carrier mobility of the trivial γ and Weyl β bands as a function of temperature.

among magnetic topological semimetals [30] that are testament to the low defect concentration in our single-crystalline samples.

It is helpful to consider the Hall effect in the context of Shubnikov–de Haas oscillations, which serve as a caliper for the Fermi surface cross-sectional area [31]. From the oscillation analysis, and consistent with Ref. [22], the carrier densities of the trivial γ Fermi surface pocket, and of β with linear Weyl dispersion, are estimated as 6.6×10^{19} cm^{-3} and 1.0×10^{19} cm^3, close to n_1 and n_2 from the Hall effect (see Supplemental Material [26]). We conclude that the electrical Hall effect in NdAlSi is dominated by two hole-type Fermi surfaces: the trivial γ pocket with carrier density n_1 and the low-mass Weyl electrons of β with carrier density n_2 and exceedingly high carrier mobility μ_2. Our main point of interest, the Weyl fermions in the Σ pocket, may also represent a minority contribution to n_2 and μ_2, but their fingerprints appear much more clearly in the thermoelectric response. All Fermi surface segments shown in Fig. 1(c) are clearly observed in quantum oscillation experiments that are well consistent with density functional theory calculations (Table S1).

B. Thermoelectric phenomena: Seebeck effect

Having established a basic understanding of electric transport in NdAlSi, we move on to the thermoelectric effects. Applying a temperature gradient $(-\partial_x T)$ to the sample, voltages appear both along the x and y axes; these voltages define the thermoelectric Seebeck and Nernst effects $S_{xx} = -E_x/|-\partial_x T|$ and $S_{xy} = E_y/|-\partial_x T|$. In Fig. 2(b), S_{xx} is divided by temperature, a common way to correct for the reduced ability of electrons to carry entropy upon cooling. The Seebeck effect is positive—consistent with the sign of the Hall effect—and S_{xx}/T is nearly independent of temperature above 50 K; a pronounced enhancement appears below 50 K, with a maximum around $T_{max} = 15$ K. Excluding the phonon-drag effect (Fig. S5), we proceed to interpret the thermoelectric phenomena in NdAlSi in terms of a thermally induced drift of charge carriers, using semiclassical transport theory. The Seebeck enhancement at T_{max} is closely related to the correlation-driven Nernst effect of Weyl electrons discussed in the following sections. Our focus here on the Hall and Nernst response of NdAlSi is motivated mostly by their enhanced sensitivity to high-mobility conduction electrons.

C. Extracting band parameters from the Nernst effect

It is well established that the thermoelectric effects S_{xx} and S_{xy} are much more sensitive to details of the electronic structure in close vicinity of the Fermi energy, as compared to electrical transport [9]. The Nernst effect is then a sensitive probe for the energy derivative of electronic band parameters in the vicinity of the Fermi edge, such as dn/dE for the carrier density and $d\tau/dE$ for the carrier relaxation time [10–17]. To separate the correlation-driven Nernst signal ΔS_{xy} originating from sizable $d\tau/dE$ in NdAlSi, we derive expressions for the thermoelectric response as a sum of various Fermi surface pockets. This kind of multiband analysis of the thermoelectric effect has rarely been attempted in the literature, e.g., for specific limiting cases in Refs. [32–35]. First, it is useful to normalize the Nernst effect by the electric resistivity ρ_{xx}; the experimental data at high and low temperatures are then well described by two terms, attributed to two Fermi surfaces γ and β,

$$\frac{S_{xy}}{\rho_{xx}T} = A_1' F(\mu_1, B) + A_2' G(\mu_2, B), \tag{1}$$

with prefactors A_1' and A_2', carrier mobilities μ_1 and μ_2, and dimensionless functions F and G for the γ and β pockets of the Fermi surface, respectively. Like the Hall conductivity F, G has pronounced maxima at intermediate magnetic fields if the carrier mobility is high. Our analysis shows that only at intermediate temperatures, an additional term ΔS_{xy} related to $d\tau/dE$ from correlations on the Σ pocket appears on top of this well-defined background; more details are given in Sec. III.

The background specified by Eq. (1), however, contains a lot of valuable information in itself, going far beyond what can be extracted from the Hall effect. Being highly nonlinear as a function of magnetic field, the Nernst signal in Fig. 3 gives the reasonable four fit parameters of Eq. (1) already at high temperature, $T > 40$ K (see also Fig. S1). A good description of the data can be obtained even when fixing the ratios $A_1'/A_2' = 7.0$ and $\mu_2/\mu_1 = 3.1$ for the entire data set, independent of temperature; the corresponding fit is shown by black dashed lines in Figs. 3(a) and 3(b). Encouragingly, the extracted carrier mobilities are close to the values in Fig. 2(c). The prefactors A_1' and A_2', meanwhile, are directly related to dn/dE, that is, to the effective band mass m_γ of γ and Fermi velocity v_β of β; these cannot be extracted from the Hall effect alone. Figures 3(i) and 3(j) show m_γ and v_β to be nearly independent of temperature, taking values of 0.25 m_0 (m_0 being the free electron mass) and 6.0×10^5 m/s, respectively, in quantitative agreement with our analysis of quantum oscillations at low temperatures (Figs. S2 and S3; Table S1).

We further demonstrate that Eq. (1), without additional ΔS_{xy}, describes the experimental observations well at the lowest temperatures, deep in the magnetically ordered state. The ΔS_{xy} term found in the temperature range 10 K to 30 K appears to be absent at the lowest temperatures. Extrapolating the band parameters A_1', A_2', μ_1, and μ_2 as in Sec. III, we find an excellent, parameter-free description of the experimental data at $T = 2$ K; see Fig. 3(h). It is emphasized that, although the curve at the low temperature in Fig. 3(h) shows a sharp, steplike anomaly, this observation is not attributed to an anomalous Nernst effect from

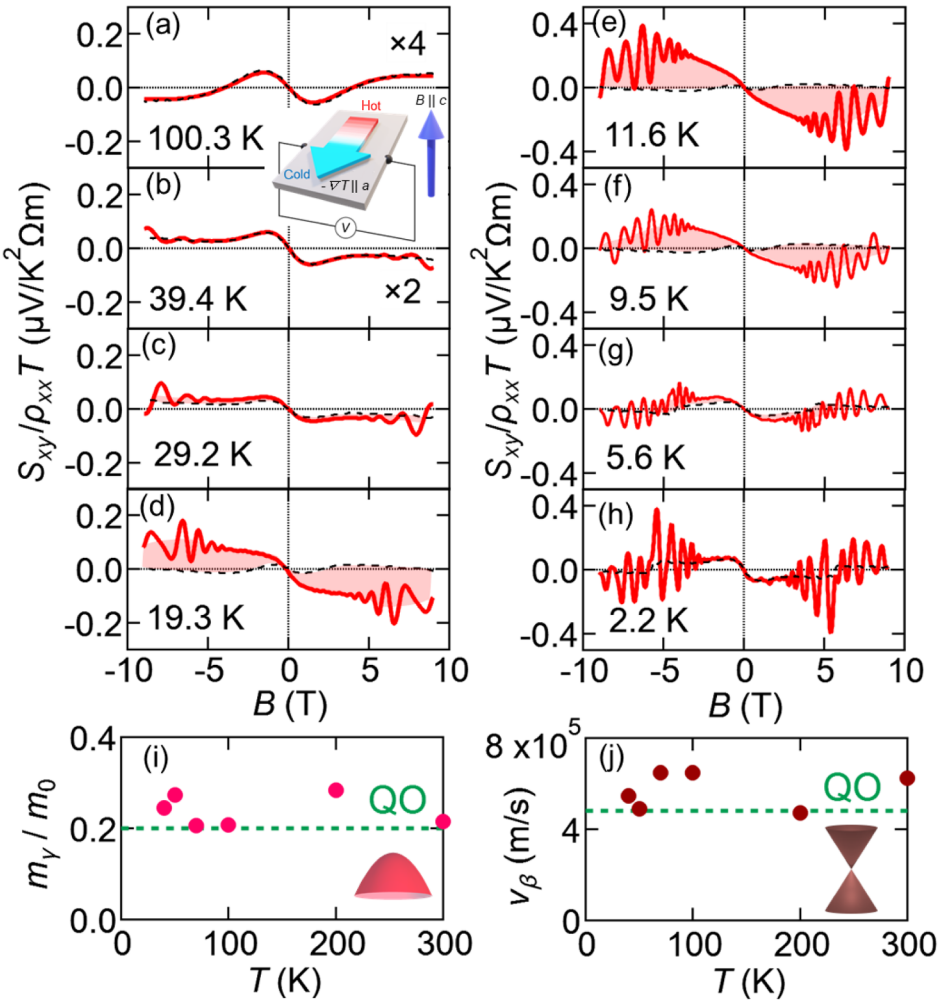

FIG. 3. Two-carrier analysis of the thermoelectric Nernst effect in NdAlSi. (a)–(h) Magnetic field dependence of Nernst effect S_{xy} normalized by resistivity and temperature. Two-carrier decomposition of the Nernst effect is shown by black dotted lines; this represents a fit to Eq. (1) at $T \geq 35$ K and a calculated curve according to Eq. (1), with extrapolated model parameters, at lower temperatures. An excess Nernst signal ΔS_{xy}, beyond Eq. (1), appears at intermediate temperatures $T = 10 - 30$ K, marked by pale red shading between the data and the semiclassical calculation. Inset: sample geometry for thermoelectric measurements, where the magnetic field and temperature gradient are applied along the crystallographic c and a axes, respectively. (i),(j) Temperature dependence of effective mass and Fermi velocity for γ and β pockets with quadratic and linear band dispersions, respectively. Corresponding electronic structure parameters estimated from quantum oscillation experiments are also shown as green dotted lines in panels (i) and (j).

spin-orbit interactions [36], but it can be explained by a conventional two-carrier model. Instead, the semiclassical Lorenz force acting on drifting, high-mobility charge carriers in a magnetic field quantitatively explains the data. Significant deviations from Eq. (1) appear below 30 K, shown by red shaded areas in Figs. 3(c)–3(g), with the implication of an additional contribution ΔS_{xy} originating from relaxation time effects ($d\tau/dE$), strongly enhanced just above the Néel transition at $T_N = 7.4$ K.

D. Nernst effect by scattering from magnetic fluctuations

Why should the additional term ΔS_{xy} be ascribed to $d\tau/dE$ and thus to a magnetic instability driven by correlations of the electron gas in NdAlSi? We offer five pieces of evidence based on the profiles of $\Delta S_{xy}/\rho_{xx}T$ in Fig. 4, viewed in the context of *ab initio* band-theory calculations. First, the field-dependent profile $\Delta S_{xy}(B)$ is suppressed by increasing the field beyond 3–5 T. Such a signal cannot arise from the anomalous Nernst effect that is in proportion to the bulk magnetization [4–8]. Second, our analysis shows that $\Delta S_{xy}(B)$ is not likely due to additional enhancement of A_1' or A_2' since no anomaly appears in the carrier density and mobility around T_N [Figs. 2(b) and 2(c)]. Third, the fact that ΔS_{xy} drops sharply at low temperature indicates that a potential change of the electronic band dispersion, e.g., due to zone folding in the magnetically ordered state, cannot be its root cause. In addition, this suppression suggests that a contribution from the anomalous Nernst effect due to Berry curvature of the

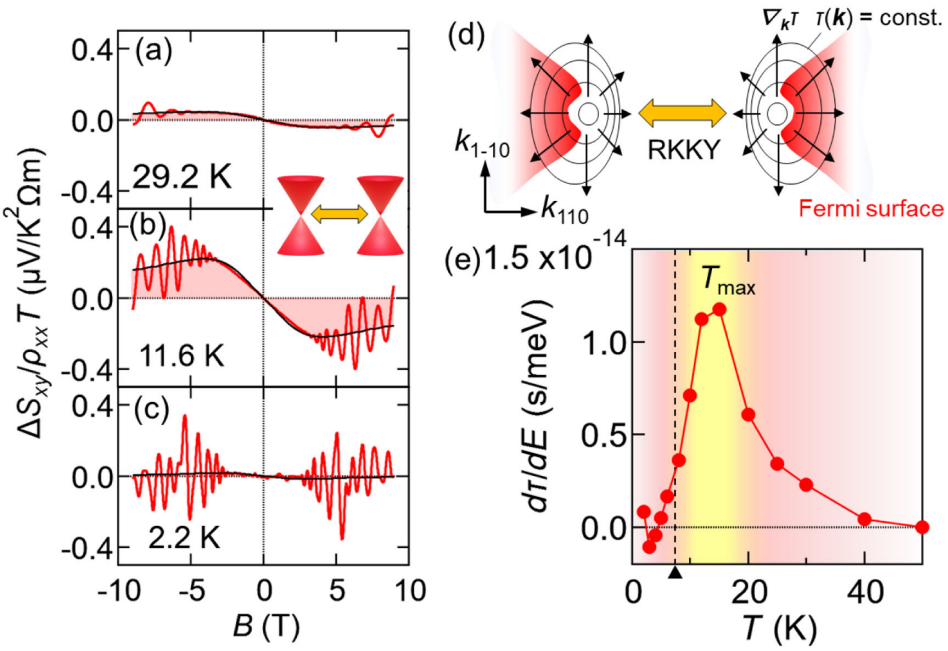

FIG. 4. Enhancement of thermoelectric Nernst effect due to electron correlations from a magnetic Fermi surface instability. (a)–(c) Magnetic field dependence of excess Nernst signal ΔS_{xy}, normalized by temperature and longitudinal resistivity ρ_{xx}, at 30 K, 12 K, and 2 K. A fit to Eq. (2) is indicated by the black line. (d) Illustration: contour lines of relaxation time $\tau(\mathbf{k})$ in momentum space with a hot spot of $\tau(\mathbf{k})$, such as can be driven by magnetic ordering with the propagation vector $\mathbf{Q} \approx (2/3, 2/3, 0)$ in NdAlSi, cf. Fig. 1. The arrows indicate a $\mathbf{k}$-space gradient of the relaxation time. For a given electron or hole on the Fermi surface, the effective energy dependence of τ is a product of this gradient and the inverse Fermi velocity, $d\tau/dE = d\tau/d\mathbf{k} \cdot d\mathbf{k}/dE$. (e) Energy derivative of carrier relaxation time $d\tau/dE$, derived from ΔS_{xy} and attributed to correlations on the Σ pocket. Yellow shading and a vertical dashed line mark the regime of strong fluctuations and the transition to long-range magnetic order at $T_N = 7.4$ K, respectively.

topological band structure is unlikely [36]. Fourth, a scaling analysis of the Nernst effect as a function of magnetization in Fig. S4 rules out a competing scenario, where ΔS_{xy} is driven by the emergent magnetic field of spin fluctuations with left- or right-handed spin chirality [37–40]. Fifth and finally, we are able to describe ΔS_{xy} in semiclassical theory by the expression

$$\frac{\Delta S_{xy}}{\rho_{xx}T} = B_3\left(\frac{\pm 2\mu_3 B - \tan\theta_H(1-(\mu_3 B)^2)}{(1+(\mu_3 B)^2)^2}\right), \qquad (2)$$

where μ_3, $\tan\theta_H = \rho_{yx}/\rho_{xx}$, and $B_3 \propto d\tau/dE$ are the carrier mobility, the (total) Hall angle, and a prefactor independent of the magnetic field, respectively (see Sec. III). Fits of ΔS_{xy} to Eq. (2) are shown as black dashed lines in Figs. 4(a)–4(c). On a quantitative level, we find $\mu_3/\mu_2 = 0.6$, consistent with the calculated ratio of Fermi velocities v_Σ and v_β of the two Weyl-type Fermi surfaces illustrated in Fig. 1(c).

Figure 4(e) shows the temperature-dependent profile of $d\tau/dE$ obtained from B_3, with a sharp maximum at $T_{max} = 15$ K, implying characteristic broadening of the Fermi-Dirac distribution of $3.8k_B T_{max} \sim 3$ millielectron volts (meV); see Fig. S6. Figure 1(d) demonstrates consistency between this observation and the calculated band-filling dependence of the Weyl-type Σ pocket, where the Fermi contour at $E_F = -3$ meV just barely touches the yellow nesting plane, a hot spot of electron scattering introduced by the (fluctuating) magnetic order. Note that the sign $d\tau/dE > 0$ indicates enhanced scattering of charge carriers below the Fermi energy.

E. Discussion

We argue above that the additional signal ΔS_{xy}, appearing in a limited window of temperature, should be ascribed to charge carrier correlations and suppressed carrier relaxation time in proximity to a Fermi surface nesting instability. More quantitatively, the total relaxation rate of electrons is a sum of various terms according to Matthiessen's rule [9], with $\tau^{-1}(\mathbf{k}) = \tau_0^{-1} + \tau_{ph}^{-1} + \tau_{el\text{-}el}^{-1} + \tau_{el\text{-}m}^{-1}(\mathbf{k}) + \ldots$, where τ_0, τ_{ph}, and $\tau_{el\text{-}el}$ represent scattering from lattice defects, lattice vibrations, and electron-electron interactions, respectively (see Supplemental Material [26]). We assume, for simplicity, that only scattering of conduction electrons from magnetic fluctuations $\tau_{el\text{-}m}$ depends on the position $\mathbf{k}$ of an electronic state in momentum space. Then, the energy derivative that enters the formula for the Nernst effect is written as $d\tau/dE = d\tau/d\mathbf{k} \times d\mathbf{k}/dE$, and the latter factor is proportional to the inverse Fermi velocity $\mathbf{v}_F$. The derivative, and hence ΔS_{xy}, becomes large when scattering from fluctuations constitutes a sizable portion of $\tau^{-1}(\mathbf{k})$, i.e., in clean materials

TABLE I. Carrier mobility μ and energy derivative of the carrier relaxation time τ for correlated materials with lifetime enhancement of the thermoelectric effect. The energy derivative of $\mu \sim \tau/E_F$ has two components, from the relaxation time and the Fermi energy, shown in the third and fourth columns, respectively [12–17]. Materials with small Fermi surfaces and high carrier mobility, such as PbSnSe, have sizable filling dependence of μ even in the absence of correlations. Among correlated materials with unconventional Nernst responses, NdAlSi shows exceedingly high mobility, which enables us to perform a quantitative analysis of $|\mathrm{dln}(\tau)/dE|$ with resolution in momentum space. Three centerdots indicate that the data is not available, while "Y" and "N" represent if the Seebeck and Nernst effects are measured in the reference or not.

Material	μ ($\mathrm{cm}^2/\mathrm{Vs}$)	$\lvert\mathrm{dln}(\tau)/dE\rvert$ (eV^{-1})	$\lvert\mathrm{dln}(E_F)/dE\rvert$ (eV^{-1})	S_{xx}	S_{xy}	Reference
NdAlSi, β	6000	⋯	7	Y	Y	This work
NdAlSi, Σ	3500	33	12	Y	Y	This work
PbSnSe	100,000	⋯	20	Y	Y	[17]
$Co_{0.999}Ni_{0.001}Sb_3$	200	650	⋯	Y	Y	[12]
$CeCu_2Si_2$	80	150	⋯	Y	Y	[13]
$CuFeS_2$	60	680	⋯	Y	N	[14]
$Mo_{0.92}Nb_{0.08}Te_2$	40	110	⋯	Y	N	[15]
MnGe	∼5	10	⋯	Y	N	[16]

with high carrier mobility. Figure 4(d) illustrates contour lines of the relaxation time $\tau(\mathbf{k})$ in momentum space, with a hot spot of $\tau(\mathbf{k})$ that can be driven by magnetic fluctuations with propagation vector $\mathbf{Q} \approx (2/3, 2/3, 0)$ in NdAlSi.

Then, the essential ingredients for large Nernst signals in the present mechanism are (a) strong or at least moderately strong coupling between the electron gas and other (collective) degrees of freedom, impacting the carrier relaxation time and (b) the presence of conducting carriers with high mobility μ. Although (b) is not exclusive to Weyl or Dirac electrons, or even to topological semimetals as a material class, the Σ pocket in NdAlSi can serve well as a toy model system, where relaxation time effects enhance the thermoelectric Nernst voltage.

Cooling below $T_{\max} = 15$ K, all Weyl electrons of the Σ pocket are now removed from the nesting hot spot by more than the width of the Fermi-Dirac distribution. These electrons cannot participate in enhanced scattering from magnetic correlations—see Fig. 1(d)—and ΔS_{xy} begins to drop rapidly. The effect of $d\tau/dE$ on the thermoelectric Seebeck effect has been suggested in some recent works [11–18], while related phenomena in the Nernst effect remain largely unexplored. The existing literature is summarized in Table I, which highlights the present Weyl semimetal NdAlSi's unique combination of high carrier mobility and sizable $d\tau/dE$. Sharp features in the Nernst signal $S_{xy}(B)$ of NdAlSi thus reveal a small minority of high-mobility Weyl electrons, exposed to electron correlations by a Fermi surface nesting instability.

Recent insights into the materials engineering of topological matter have led to the identification of chiral and polar materials with robust linear band crossing points [21,25], to which correlations can be introduced via chemical composition tuning while leaving intact the fundamental symmetries of the crystalline space group—and maintaining band degeneracies. The resulting high-mobility, correlated semimetals represent a family of weakly coupled materials that stand apart from the more established copper-oxide and iron-based superconductors [41–45], from layered chalcogenides with charge-density wave instabilities [46], or from heavy-fermion compounds [47]. For example, in the much more strongly correlated copper oxides, the interpretation of the thermoelectric Nernst effect [48–50] and the notion of hot spots of relaxation time on the Fermi surface [43] remain controversial. In contrast, NdAlSi and its relatives likely realize the weak-coupling scenario of Ruderman, Kittel, Kasuya, and Yosida [27–29], where the momentum-dependent self-energy, or relaxation time $\tau(\mathbf{k})$, is calculated in first-order perturbation theory about $\int d^3\mathbf{q}\, G(\mathbf{q})\chi(\mathbf{k}-\mathbf{q})$ from the electronic Green's function G and the magnetic susceptibility $\chi(\mathbf{q})$. However, the present mechanism of an enhanced Nernst effect based on relaxation time engineering is generally applicable, providing a stimulus to investigate thermoelectric effects in as-yet less-explored metallic materials, including clean systems with nesting instabilities such as elemental Cr or the RTe_3-layered CDW systems (R = rare earth). In fact, we found an enhanced Nernst signal due to the relaxation time effect in another high-mobility semimetal, GdPtBi (see Supplemental Material [26]), suggesting that enhancements of the thermoelectric response commonly appear in various correlated materials due to magnetic fluctuations close to the magnetic transition temperature. Even for the anomalous Nernst effect, previous work suggests a correlation of magnetic entropy (fluctuations) and the amplitude of the signal [51]. The present enhanced Nernst effect is particularly pronounced in crystals with high carrier mobility and low impurity concentration, criteria that are often fulfilled for large single-crystalline grains; yet, even some polycrystalline materials can have very high carrier mobilities as well as large thermoelectric responses [52–54]. In addition, the relaxation time effect $d\tau/dE$ also has an impact not only on the Nernst effect but also on the Seebeck effect, which can

be operated without the application of the magnetic field. In this way, thermoelectric phenomena generated via the relaxation time of charge carriers open a window into the fundamental physics of electron correlation—but may also find real-world applications in energy harvesting using highly conductive metals, where conduction electrons are coupled to collective spin, orbital, or lattice fluctuations.

III. METHODS

A. Sample preparation and characterization

Single-crystalline samples of NdAlSi were prepared by the Al flux method. Elemental Nd, Si, and Al elements were inserted into an Al_2O_3 crucible and sealed inside a quartz tube in vacuum. The starting composition (Nd∶Si∶Al) was 1∶1∶10. The tube was placed in a box furnace, heated from room temperature to 1000 °C in 5 hours, and kept there for 12 hours.

Subsequently, it was slowly cooled to 700 °C in 50 hours (−6 °C/h) and kept for 12 hours. The crucible was quickly removed from the furnace and centrifuged. Millimeter-sized, platelike crystals with the c axis normal to the sample plane and the a axis parallel to the plate's edges were obtained, which are characterized by sharp, Laue x-ray diffraction patterns.

B. Thermoelectric measurements

Thermoelectric measurements on NdAlSi were performed in high vacuum ($<1\times10^{-4}$ Torr) using a Quantum Design Physical Property Measurement System (PPMS). The sample was fixed by Ag paste (Dupont) to a Cu block, which serves as a heat sink. The Cu block is attached to the sample pack by using low-temperature adhesive (GE varnish). Thermal gradients were applied by applying current to a 1 kΩ chip resistor, and temperature gradients on the rectangular-shaped sample (about 0.5 K/mm) were read by Nickel-Chromium/Constantan thermocouples. The thermocouples were attached to a thick gold wire by Stycast 2850FT epoxy, and the thick Au wire in turn was attached to the side of the sample by silver paste. The thermoelectric voltage drop was measured through phosphor bronze wires (40 μm in diameter) attached to the side of the sample. The entire setup was covered by a copper tube to prevent radiative heating from outside.

C. *Ab initio* band calculations

We performed spin density functional theory calculations in the ferromagnetic state of NdAlSi using the Vienna *ab initio* simulation package [55]. We employed the exchange-correlation functional proposed by Perdew, Burke, and Ernzerhof [56] and pseudopotentials with the projector augmented wave basis [57,58], and used the experimental lattice parameters $a=4.1972$ Å and $c=14.4915$ Å [22]. The Hubbard U correction with $U=6.0$ eV for Nd-4f states and spin-orbit interactions were taken into account. A 16^3 Monkhorst-Pack k grid and 500 eV as a plane-wave cutoff were used for the self-consistent calculations. Then, we constructed a tight-binding model using the WANNIER90 package [59]. Here, 144 Bloch states were evaluated on a 8^3 uniform $\mathbf{k}$ grid. The trial orbitals were set to be Nd-f and d, Al-s and p, as well as Si-s and p orbitals. Fermi surface calculations were performed using a 240^3 uniform $\mathbf{k}$ grid based on the abovementioned tight-binding model.

D. Mott relation and energy derivative of carrier relaxation time

The electric and thermoelectric conductivity tensors define a material's current $J_i=\sigma_{ij}E_j$ and $J_i=\alpha_{ij}(-\partial_j T)$ in response to an applied electric field E_j and to a temperature gradient $(-\partial_j T)$, respectively. Expressions for σ_{ij}, α_{ij} in a magnetic field are derived using semiclassical Boltzmann theory (9):

$$-\frac{\partial f_0}{\partial\varepsilon}\left[\left(\frac{\partial\zeta}{\partial\mathbf{x}}+\frac{\varepsilon-\zeta}{T}\frac{\partial T}{\partial\mathbf{x}}\right)\cdot\mathbf{v}-e\mathbf{E}\cdot\mathbf{v}\right]+\frac{\partial g_{\mathbf{k}}}{\partial\mathbf{k}}\cdot(\mathbf{v}\times\mathbf{B})=-\frac{g_{\mathbf{k}}}{\tau}. \tag{3}$$

Here, $g_{\mathbf{k}}$ corresponds to a distortion of the equilibrium probability for occupying each quantum state, described by the Fermi-Dirac distribution function f_0. Furthermore, ε, ζ, $\mathbf{v}$, and τ are the electronic band dispersion, chemical potential, Fermi velocity, and carrier relaxation time, respectively. The magnetic field $\mathbf{B}$ is applied along $\mathbf{z}$, and the electric field $\mathbf{E}$ is parallel to $\mathbf{x}$. We neglect any spatial dependence of $g_{\mathbf{k}}$, as well as Berry phase contributions. Integrating over all Fermi surface sheets, we derive the electric and thermoelectric currents as

$$\mathbf{J}_{\mathrm{el}}=e^2\sum_{\mathrm{bands}}\int\frac{d^3\mathbf{k}}{(2\pi)^3}\left(\frac{\partial f_0}{\partial\varepsilon}\right)\left[\left(\frac{\mathbf{v}-\frac{e\tau}{m}\mathbf{v}\times\mathbf{B}}{1+(\frac{e\tau}{m})^2B^2}\right)\cdot\mathbf{E}\right]\tau_{\mathbf{k}}\mathbf{v}, \tag{4}$$

$$\mathbf{J}_{\mathrm{th-el}}=e\sum_{\mathrm{bands}}\int\frac{d^3\mathbf{k}}{(2\pi)^3}\left(\frac{\partial f_0}{\partial\varepsilon}\right)\left(\frac{\varepsilon-\zeta}{T}\right)\times\left[\left(\frac{\mathbf{v}-\frac{e\tau}{m}\mathbf{v}\times\mathbf{B}}{1+(\frac{e\tau}{m})^2B^2}\right)\cdot\frac{\partial T}{\partial\mathbf{x}}\right]\tau_{\mathbf{k}}\mathbf{v}. \tag{5}$$

The latter expression is further approximated by the crucial insight of Mott, who reduced the energy factor $(\varepsilon-\zeta)$ in Eq. (5) to an energy derivative over the other integrands [9]. The final expression depends on the energy derivative of the carrier density, i.e., of the partial density of states, as well as the energy derivative of $\tau_{\boldsymbol{k}}$. The latter is the main focus of the present work. Note that the assumption of a unique value of $\tau_{\boldsymbol{k}}$ for Σ is a necessary but crude approximation, in the case of the hot-spot scenario discussed in the main text.

E. Normal Nernst effect for more than one electronic band

Consider the electric field **E** caused by the diffusion of charge carriers in a thermal gradient ∇T along **x** and a magnetic field **B** along **z**. The sign of the Nernst effect is then fixed by the convention that diffusion of superconducting vortices causes a positive S_{xy}, $S_{xy} = E_y/|\nabla T|$ [17,48]. Generally, the Nernst effect can have contributions from the orbital motion of carriers, from spin-orbit interactions in conjunction with the net magnetization **M** of the solid, and from higher-order terms—for example, from the spin chirality $\mathbf{S}_i \cdot (\mathbf{S}_j \times \mathbf{S}_k)$. These effects are dubbed normal, anomalous, and topological Nernst effects, respectively. In the semiclassical regime and using the relaxation time approximation with isotropic τ, the normal Nernst signal is expressed as

$$S_{xy} = -\frac{\pi^2}{3}\frac{k_B^2}{e} T \rho_{xx}\sigma_{xx}\frac{\partial \tan\theta_H}{\partial \varepsilon}. \tag{6}$$

Here, $\tan\theta_H = \sigma_{xy}/\sigma_{xx}$ is the Hall angle. Furthermore, consider the Drude expressions for multiband conduction, $\sigma_{xx} = \Sigma_i e|n_i|\mu_i/[1+(\mu_i B)^2]$ and $\sigma_{xy} = \Sigma_i e n_i \mu_i^2 B/[1+(\mu_i B)^2]$, with carrier densities n_i and carrier mobilities $\mu_i = e\tau_i/m_i$; $e > 0$ and m_i are the fundamental charge and the effective band masses, respectively. By transposing T and ρ_{xx} to the left side, and transforming the remaining right-hand side of Eq. (6), we derive

$$\frac{S_{xy}}{\rho_{xx}T} = \sum_i \left[A_i \left(\frac{\pm\mu_i B - \tan\theta_H}{1+(\mu_i B)^2} \right) + B_i \left(\frac{\pm 2\mu_i B - \tan\theta_H (1-(\mu_i B)^2)}{(1+(\mu_i B)^2)^2} \right) \right]. \tag{7}$$

The upper and lower sign notations describe hole- and electron-type carriers, respectively. Here, $A_i = -\pi^2 k_B^2 \mu_i/3 \cdot dn_i/dE$ and $B_i = -\pi^2 k_B^2 n_i/3 \cdot d\mu_i/dE$ are the contributions from the energy derivatives of the carrier density and of the carrier mobility. Furthermore, by decomposing contributions from quadratic bands ($E_i^Q = \hbar^2 k_i^2/2m_i$) and linear bands ($E_i^L = \hbar k_i v_i$, while replacing $m_i \to E_{Fi}/v_{Fi}^2$ in the expression for the mobility), the following relation can be derived:

$$\frac{S_{xy}}{\rho_{xx}T} = \sum_{i:\,\mathrm{Quad}} \left[A_i^Q \left(\frac{\pm\mu_i B - \tan\theta_H}{1+(\mu_i B)^2} \right) + B_i^Q \left(\frac{\pm 2\mu_i B - \tan\theta_H (1-(\mu_i B)^2)}{(1+(\mu_i B)^2)^2} \right) \right] + \sum_{i:\,\mathrm{Line}} \left[A_i^L \left(\frac{\pm\mu_i B - \tan\theta_H}{1+(\mu_i B)^2} \right) + \left(\frac{A_i^L}{3} + B_i^L \right) \left(\frac{\pm 2\mu_i B - \tan\theta_H (1-(\mu_i B)^2)}{(1+(\mu_i B)^2)^2} \right) \right]. \tag{8}$$

Here, the coefficients for quadratic bands are $A_i^Q = \pm g_s g_d k_B^2 \mu_i m_i k_i/6\hbar^2$ and $B_i^Q = -g_s g_d e k_B^2 k_i^3/18 m_i \cdot d\tau_i/dE$; the coefficients for linear bands are $A_i^L = \pm g_s g_d k_B^2 \mu_i k_i^2/6\hbar v_i$ and $B_i^L = -g_s g_d e k_B^2 v_i k_i^2/18\hbar \cdot d\tau_i/dE$, where g_s and g_d are the spin and orbital degeneracy of each Fermi surface pocket, respectively.

In the specific case of NdAlSi, the Nernst effect at high and low temperatures is well described by parallel conduction of a trivial hole pocket γ ($E_\gamma = \hbar^2 k_\gamma^2/2m_\gamma$) and a Weyl-type hole pocket β ($E_\beta = \hbar k_\beta v_\beta$). At intermediate temperatures, additional contributions to S_{xy} that are not from the energy-dependent carrier density are summarized in the term $\Delta S_{xy}/\rho_{xx}T$,

$$\frac{S_{xy}}{\rho_{xx}T} = A_\gamma \left(\frac{\pm\mu_\gamma B - \tan\theta_H}{1+(\mu_\gamma B)^2} \right) + A_\beta \left(\frac{\pm\mu_\beta B(5+3(\mu_\beta B)^2) - 2\tan\theta_H (2+1(\mu_\beta B)^2)}{3(1+(\mu_\beta B)^2)^2} \right) + \frac{\Delta S_{xy}}{\rho_{xx}T}, \tag{9}$$

where the coefficients are $A_\gamma = \pm g_s g_d k_B^2 \mu_\gamma m_\gamma k_\gamma/6\hbar^2$ and $A_\beta = \pm g_s g_d k_B^2 \mu_\beta k_\beta^2/6\hbar v_\beta$. Here, we define $A'_\gamma = A_\gamma/\mu_\gamma$ and $A'_\beta = A_\beta/\mu_\beta$. We set the spin and orbital degeneracies of γ (β) to $g_s = 2$ ($g_s = 1$) and $g_d = 4$ ($g_d = 4$), respectively, for the analysis at high temperatures, which is consistent with the large spin-orbit splitting of β in the nonmagnetic state of polar NdAlSi.

We obtain an excellent description of S_{xy} using Eq. (9) with four free parameters (A'_γ, A'_β, μ_γ, and μ_β) at high temperatures above 40 K. However, features in S_{xy} become

less sharp at $T > 70$ K, so a reduction in the number of free parameters was found to be helpful to stabilize the fit. We fix the ratios $A'_\gamma/A'_\beta \sim 7.0$ and $\mu_\beta/\mu_\gamma \sim 3.1$ independent of T, retaining a very good description of the experimental data. In particular, all parameters extracted from the semiclassical model of S_{xy} have distinct physical meaning and can be cross-referenced with the Hall effect and quantum oscillation experiments.

We extended the analysis according to Eq. (9) to $T < 40$ K by extrapolating the band parameters A'_γ, A'_β, μ_γ, and μ_β as follows. First, $A'_\beta = \pm g_s g_d k_B^2 \hbar k_\beta^2/v_\beta$ was set to 0.45 independent of temperature, as changes of the electronic structure are moderate in this regime [see Figs. 2(b) and 3(j)]. In addition, the carrier mobilities were extrapolated to low T, being proportional to the longitudinal conductivity σ_{xx}. Furthermore, we assumed that the spin degeneracy (g_s) of the γ pocket smoothly changed from unity at 2 K to $g_s = 2$ at 40 K, considering that the exchange splitting of electronic bands is enhanced at low temperatures. Meanwhile, g_s of β was set to unity at all temperatures, reflecting its small Fermi surface volume and large spin-orbit splitting even in the paramagnetic state. In this way, we estimated the first and second terms in Eq. (9) and isolated ΔS_{xy} at intermediate temperatures.

F. Two-carrier fit of the Hall conductivity

We modeled the Hall conductivity σ_{xy} with a two-carrier Drude expression as [9]

$$\sigma_{xy} = n_1 e\mu_1 \frac{\mu_1 B}{1+(\mu_1 B)^2} + n_2 e\mu_2 \frac{\mu_2 B}{1+(\mu_2 B)^2}. \quad (10)$$

Here, n_1 and n_2 (μ_1 and μ_2) are the carrier densities (carrier mobilities). The resulting carrier densities n_1 and n_2 show good agreement with quantum oscillations of the γ and β pockets, as discussed in the main text.

Note added. Recently, we became aware of a related work focused on quantum oscillations in RAlSi (R = rare earth) [60].

ACKNOWLEDGMENTS

We acknowledge H. Isobe, K. Ueda, N. Nagaosa, and T.-h. Arima for fruitful discussion. This work was supported by JSPS KAKENHI Grants No. JP21K13877, No. JP22H04463, No. JP22K20348, No. JP23H05431, and No. 23K13057, as well as JST CREST Grants No. JPMJCR1874 and No. JPMJCR20T1 (Japan), JST FOREST Grant No. JPMJFR2238 (Japan), and JST-PREST Grant No. JPMJPR20L7. The authors are grateful for support by the Fujimori Science and Technology Foundation, the New Materials and Information Foundation, the Murata Science Foundation, the Mizuho Foundation for the Promotion of Sciences, the Yamada Science Foundation, the Hattori Hokokai Foundation, the Iketani Science and Technology Foundation, the Mazda Foundation, the Casio Science Promotion Foundation, the Takayanagi Foundation, the Foundation for Promotion of Material Science and Technology of Japan (MST Foundation), and the Yashima Environment Technology Foundation.

R. A., Y. Ta, Y. To., and M. H. conceived and supervised the project. R. Y. and A. K. synthesized and characterized the single crystals. R. Y., T. T., and M. H. carried out and analyzed the electrical and thermoelectric transport measurements. R. Y., A. M., and M. T. conducted tunnel diode oscillator (TDO) measurements under high magnetic fields. T. N. and R. A. performed *ab initio* calculations. R. Y. and M. H. wrote the manuscript, with the support of T. N. and R. A. All authors discussed the results and commented on the manuscript.

The authors declare no competing interests.

[1] Y. S. Hor, A. Richardella, P. Roushan, Y. Xia, J. G. Checkelsky, A. Yazdani, M. Z. Hasan, N. P. Ong, and R. J. Cava, *p-type* Bi_2Se_3 *for topological insulator and low temperature thermoelectric applications*, Phys. Rev. B **79**, 195208 (2009).

[2] L.-D. Zhao, G. Tan, S. Hao, J. He, Y. Pei, H. Chi, H. Wang, S. Gong, H. Xu, V. P. Dravid, C. Uher, G. J. Snyder, C. Wolverton, and M. G. Kanatzidis, *Ultrahigh power factor and thermoelectric performance in hole-doped single-crystal* SnSe, Science **351**, 141 (2015).

[3] T. C. Harman, J. M. Honig, S. Fischler, A. E. Paladino, and M. Jane Button, *Oriented single-crystal bismuth Nernst-Ettingshausen refrigerators*, Appl. Phys. Lett. **4**, 77 (1964).

[4] M. Mizuguchi and S. Nakatsuji, *Energy-harvesting materials based on the anomalous Nernst effect*, Sci. Technol. Adv. Mater. **20**, 262 (2019).

[5] M. Ikhlas, T. Tomita, T. Koretsune, M.-T. Suzuki, D. Nishio-Hamane, R. Arita, Y. Otani, and S. Nakatsuji, *Large anomalous Nernst effect at room temperature in a chiral antiferromagnet*, Nat. Phys. **13**, 1085 (2017).

[6] A. Sakai, Y. P. Mizuta, A. A. Nugroho, R. Sihombing, T. Koretsune, M.-T. Suzuki, N. Takemori, R. Ishii, D. Nishio-Hamane, R. Arita, P. Goswami, and S. Nakatsuji, *Giant anomalous Nernst effect and quantum-critical scaling in a ferromagnetic semimetal*, Nat. Phys. **14**, 1119 (2018).

[7] A. Sakai, S. Minami, T. Koretsune, T. Chen, T. Higo, Y. Wang, T. Nomoto, M. Hirayama, S. Miwa, D. Nishio-Hamane, F. Ishii, R. Arita, and S. Nakatsuji, *Iron-based binary ferromagnets for transverse thermoelectric conversion*, Nature (London) **581**, 53 (2020).

[8] Y. Pan, C. Le, B. He, S. J. Watzman, M. Yao, J. Gooth, J. P. Heremans, Y. Sun, and C. Felser, *Giant anomalous Nernst*

signal in the antiferromagnet $YbMnBi_2$, Nat. Mater. **21**, 203 (2022).
[9] J. M. Ziman, *Principles of the Theory of Solids* (Cambridge University Press, Cambridge, England, 1972).
[10] K. Behnia, *What is measured when measuring a thermoelectric coefficient?*, C.R. Phys. **23**, 25 (2022).
[11] K. Behnia, M.-A. Méasson, and Y. Kopelevich, *Nernst effect in semimetals: The effective mass and the figure of merit*, Phys. Rev. Lett. **98**, 076603 (2007).
[12] P. Sun, B. Wei, J. Zhang, J. M. Tomczak, A. M. Strydom, M. Søndergaard, B. B. Iversen, and F. Steglich, *Large Seebeck effect by charge-mobility engineering*, Nat. Commun. **6**, 7475 (2015).
[13] P. Sun and F. Steglich, *Nernst effect: Evidence of local Kondo scattering in heavy fermions*, Phys. Rev. Lett. **110**, 216408 (2013).
[14] H. Xie, X. Su, T. P. Bailey, C. Zhang, W. Liu, C. Uher, X. Tang, and M. G. Kanatzidis, *Anomalously large Seebeck coefficient of* $CuFeS_2$ *derives from large asymmetry in the energy dependence of carrier relaxation time*, Chem. Mater. **32**, 2639 (2020).
[15] H. Sakai, K. Ikeura, M. S. Bahramy, N. Ogawa, D. Hashizume, J. Fujioka, Y. Tokura, and S. Ishiwata, *Critical enhancement of thermopower in a chemically tuned polar semimetal* $MoTe_2$, Sci. Adv. **2**, e1601378 (2016).
[16] Y. Fujishiro, N. Kanazawa, T. Shimojima, A. Nakamura, K. Ishizaka, T. Koretsune, R. Arita, A. Miyake, H. Mitamura, K. Akiba, M. Tokunaga, J. Shiogai, S. Kimura, S. Awaji, A. Tsukazaki, A. Kikkawa, Y. Taguchi, and Y. Tokura, *Large magneto-thermopower in* MnGe *with topological spin texture*, Nat. Commun. **9**, 408 (2018).
[17] T. Liang, Q. Gibson, J. Xiong, M. Hirschberger, S. P. Koduvayur, R. J. Cava, and N. P. Ong, *Evidence for massive bulk Dirac fermions in* $Pb_{1-x}Sn_xSe$ *from Nernst and thermopower experiments*, Nat. Commun. **4**, 2696 (2013).
[18] M. Zebarjadi, S. Emad Rezaei, M. Sabbir Akhanda, and K. Esfarjani, *Nernst coecient within relaxation time approximation*, Phys. Rev. B **103**, 144404 (2021).
[19] K. K. Gomes, A. N. Pasupathy, A. Pushp, S. Ono, Y. Ando, and A. Yazdani, *Visualizing pair formation on the atomic scale in the high-*T_c *superconductor* $Bi_2Sr_2CaCu_2O_{8+\delta}$, Nature (London) **447**, 569 (2007).
[20] S.-Y. Xu *et al.*, *Discovery of Lorentz-violating type II Weyl fermions in* LaAlGe, Sci. Adv. **3**, e1603266 (2017).
[21] G. Chang *et al.*, *Magnetic and noncentrosymmetric Weyl fermion semimetals in the R*AlGe *family of compounds (*R = rare *earth)*, Phys. Rev. B **97**, 041104(R) (2018).
[22] J. Gaudet, H.-Y. Yang, S. Baidya, B. Lu, G. Xu, Y. Zhao, J. A. Rodriguez-Rivera, C. M. Hoffmann, D. E. Graf, D. H. Torchinsky, P. Nikolić, D. Vanderbilt, F. Tafti, and C. L. Broholm, *Weyl-meditated helical magnetism in* NdAlSi, Nat. Mater. **20**, 1650 (2021).
[23] N. P. Armitage, E. J. Mele, and Ashvin Vishwanath, *Weyl and Dirac semimetals in three dimensional solids*, Rev. Mod. Phys. **90**, 015001 (2018).
[24] X. Wan, A. M. Turner, A. Vishwanath, and S. Y. Savrasov, *Topological semimetal and Fermi-arc surface states in the electronic structure of pyrochlore iridates*, Phys. Rev. B **83**, 205101 (2011).
[25] G. Chang, B. J. Wieder, F. Schindler, D. S. Sanchez, I. Belopolski, S.-M. Huang, B. Singh, D. Wu, T.-R. Chang, T. Neupert, S.-Y. Xu, H. Lin, and M. Z. Hasan, *Topological quantum properties of chiral crystals*, Nat. Mater. **17**, 978 (2018).
[26] See Supplemental Material at http://link.aps.org/supplemental/10.1103/PhysRevX.14.021012 for the detailed analysis on the thermoelectric effects and quantum oscillations.
[27] M. A. Ruderman and C. Kittel, *Indirect exchange coupling of nuclear magnetic moments by conduction electrons*, Phys. Rev. **96**, 99 (1954).
[28] T. Kasuya, *A theory of metallic ferro- and antiferromagnetism on Zener's model*, Prog. Theor. Phys. **16**, 45 (1956).
[29] K. Yosida, *Magnetic properties of* Cu − Mn *alloys*, Phys. Rev. **106**, 893 (1957).
[30] M. Tanaka, Y. Fujishiro, M. Mogi, Y. Kaneko, T. Yokosawa, N. Kanazawa, S. Minami, T. Koretsune, R. Arita, S. Tarucha, M. Yamamoto, and Y. Tokura, *Topological Kagome magnet* $Co_3Sn_2S_2$ *thin flakes with high electron mobility and large anomalous Hall effect*, Nano Lett. **20**, 7476 (2020).
[31] D. Shoenberg, *Magnetic Oscillations in Metals*, 1st ed. (Cambridge University Press, Cambridge, England, 1984).
[32] Z. Zhu, X. Lin, J. Liu, B. Fauqué, Q. Tao, C. Yang, Y. Shi, and K. Behnia, *Quantum oscillations, thermoelectric coefficients, and the Fermi surface of semimetallic* WTe_2, Phys. Rev. Lett. **114**, 176601 (2015).
[33] Y. Kajikawa, *Multi-band analysis of temperature-dependent transport coefficients (conductivity, Hall, Seebeck, and Nernst) of Ni-doped* $CoSb_3$, J. Appl. Phys. **119**, 055702 (2016).
[34] Y. Kajikawa, *Analyses of low-temperature transport and thermoelectric properties of polycrystalline undoped* n − ZrNiSn, AIP Adv. **11**, 055108 (2021).
[35] I. Leahy, *Electrical, magnetic, and thermoelectric properties of semimetals*, Ph.D. Thesis, University of Colorado Boulder (2021).
[36] T. Liang, J. Lin, Q. Gibson, T. Gao, M. Hirschberger, M. Liu, R. J. Cava, and N. P. Ong, *Anomalous Nernst effect in the Dirac semimetal* Cd_3As_2, Phys. Rev. Lett. **118**, 136601 (2017).
[37] W. T. Hou, J. X. Yu, M. Daly, and J. Zang, *Thermally driven topology in chiral magnets*, Phys. Rev. B **96**, 140403 (2017).
[38] J. X. Yu, M. Daly, and J. Zang, *Thermally driven topology in frustrated systems*, Phys. Rev. B **99**, 104431 (2019).
[39] W. Wang, M. W. Daniels, Z. Liao, Y. Zhao, J. Wang, G. Koster, G. Rijnders, C.-Z. Chang, D. Xiao, and W. Wu, *Spin chirality fluctuation in two-dimensional ferromagnets with perpendicular magnetic anisotropy*, Nat. Mater. **18**, 1054 (2019).
[40] K. K. Kolincio, M. Hirschberger, J. Masell, S. Gao, A. Kikkawa, Y. Taguchi, T.-h. Arima, N. Nagaosa, and Y. Tokura, *Large Hall and Nernst responses from thermally induced spin chirality in a spin-trimer ferromagnet*, Proc. Natl. Acad. Sci. U.S.A. **118**, e2023588118 (2021).
[41] B. Keimer, S. A. Kivelson, M. R. Norman, S. Uchida, and J. Zaanen, *From quantum matter to high-temperature superconductivity in copper oxides*, Nature (London) **518**, 179 (2015).

[42] G. Sharma, C. Liu, K. Seo, J. D. Sau, and S. Tewari, *Normal-state Nernst effect from bidirectional bond density wave state in high-T_c cuprates*, Phys. Rev. B **92**, 155114 (2015).

[43] G. Grissonnanche, Y. Fang, A. Legros, S. Verret, F. Laliberté, C. Collignon, J. Zhou, D. Graf, P. A. Goddard, L. Taillefer, and B. J. Ramshaw, *Linear-in temperature resistivity from an isotropic Planckian scattering rate*, Nature (London) **595**, 667 (2021).

[44] M. Breitkreiz, P. M. R. Brydon, and C. Timm, *Transport in multiband systems with hot spots on the Fermi surface: Forward-scattering corrections*, Phys. Rev. B **89**, 245106 (2014).

[45] A. E. Koshelev, *Magnetotransport of multiple-band nearly antiferromagnetic metals due to hot-spot scattering*, Phys. Rev. B **94**, 125154 (2016).

[46] Q. H. Wang, K. Kalantar-Zadeh, A. Kis, J. N. Coleman, and M. S. Strano, *Electronics and optoelectronics of two-dimensional transition metal dichalcogenides*, Nat. Nanotechnol. **7**, 699 (2012).

[47] Q. Si and F. Steglich, *Heavy fermions and quantum phase transitions*, Science **329**, 1161 (2010).

[48] Z. A. Xu, N. P. Ong, Y. Wang, T. Kakeshita, and S. Uchida, *Vortex-like excitations and the onset of superconducting phase fluctuation in underdoped* $La_{2-x}Sr_xCuO_4$, Nature (London) **406**, 486 (2000).

[49] Y. Wang, L. Li, and N. P. Ong, *Nernst effect in high-T_c superconductors*, Phys. Rev. B **73**, 024510 (2006).

[50] J. Chang, N. Doiron-Leyraud, O. Cyr-Choinière, G. Grissonnanche, F. Laliberté, E. Hassinger, J-Ph. Reid, R. Daou, S. Pyon, T. Takayama, H. Takagi, and L. Taillefer, *Decrease of upper critical field with underdoping in cuprate superconductors*, Nat. Phys. **8**, 751 (2012).

[51] K. Geishendorf, P. Vir, C. Shekhar, C. Felser, J. I. Facio, J. van den Brink, K. Nielsch, A. Thomas, and S. T. B. Goennenwein, *Signatures of the magnetic entropy in the thermopower signals in nanoribbons of the magnetic Weyl semimetal* $Co_3Sn_2S_2$, Nano Lett. **20**, 300 (2020).

[52] S. Ishiwata, Y. Shiomi, J. S. Lee, M. S. Bahramy, T. Suzuki, M. Uchida, R. Arita, Y. Taguchi, and Y. Tokura, *Extremely high electron mobility in a phonon-glass semimetal*, Nat. Mater. **12**, 512 (2013).

[53] C. Fu, S. N. Guin, S. J. Watzman, G. Li, E. Liu, N. Kumar, V. Süß, W. Schnelle, G. Auffermann, C. Shekhar, Y. Sun, J. Gooth, and C. Felser, *Large Nernst power factor over a broad temperature range in polycrystalline Weyl semimetal* NbP, Energy Environ. Sci. **11**, 2813 (2018).

[54] T. Feng, P. Wang, Z. Han, L. Zhou, W. Zhang, Q. Liu, and W. Liu, *Large transverse and longitudinal magneto-thermoelectric effect in polycrystalline nodal-line semimetal* Mg_3Bi_2, Adv. Mater. **34**, 2200931 (2022).

[55] G. Kresse and J Furthmüller, *Efficient iterative schemes for ab initio total-energy calculations using a plane-wave basis set*, Phys. Rev. B **54**, 11169 (1996).

[56] J. P. Perdew, K. Burke, and M. Ernzerhof, *Generalized gradient approximation made simple*, Phys. Rev. Lett. **77**, 3865 (1996).

[57] P. E. Blöchl, *Projector augmented-wave method*, Phys. Rev. B **50**, 17953 (1994).

[58] G. Kresse and D. Joubert, *From ultrasoft pseudopotentials to the projector augmented wave method*, Phys. Rev. B **59**, 1758 (1999).

[59] A. A. Mostofi, J. R. Yates, Y.-S. Lee, I. Souza, D. Vanderbilt, and N. Marzari, *WANNIER90: A tool for obtaining maximally-localised Wannier functions*, Comput. Phys. Commun. **178**, 685 (2008).

[60] Q.-X. Dong, J.-F. Wang, L.-B. Zhang, J.-L. Bai, Q.-Y. Liu, J.-W. Cheng, P.-Y. Liu, C.-D. Li, J.-S. Xiang, Z.-A. Ren, P.-J. Sun, and G.-F. Chen, *Large power factor, anomalous Nernst effect, and temperature-dependent thermoelectric quantum oscillations in the magnetic Weyl semimetal* NdAlSi, Phys. Rev. B **108**, 205143 (2023).